J. Fluid Mech. (2009), *vol.* 632, *pp.* 97–107.
doi:10.1017/S0022112009007320 Printed in the United Kingdom

Separation-driven coalescence of droplets: an analytical criterion for the approach to contact

ANN LAI[1], NICOLAS BREMOND[2] AND HOWARD A. STONE[1]†

[1]School of Engineering and Applied Sciences, Harvard University, Cambridge, MA 02138, USA

[2]UPMC Paris 06, ESPCI ParisTech, CNRS UMR 7195, 10 rue Vauquelin, 75005 Paris, France

(Received 6 November 2008 and in revised form 26 March 2009)

Recent microfluidic experiments by Bremond, Thiam & Bibette (*Phys. Rev. Lett.*, vol. 100, 2008, paper no. 024501), along with simulations by Yoon *et al.* (*Phys. Fluid*, vol. 19, 2007, paper no. 102102) and near-contact experiments and simulations by Manica *et al.* (*Langmuir*, vol. 24, 2008, pp. 1381–1390), have demonstrated that two droplets can coalesce as they are separating rather than upon their collision. We analyse the experimental microfluidic flow configuration for the approach to contact with a two-dimensional model: we apply a lubrication analysis followed by the method of domain perturbation to determine the droplet deformation as a function of time. We find the approximate shape for the deformed droplet at the time of contact. In particular, for droplets of radius R, moving apart according to $h_0(t) = h_0(0) + \alpha t^2$, where $2h_0(t)$ is the separation distance, we define a non-dimensional parameter $A = 4C\mu R^2\alpha^{1/2}/\pi\gamma[h_0(0)]^{3/2}$, where μ is the viscosity of the continuous phase; γ is the interfacial tension; and C depends on the viscosity ratio between the droplets and the continuous phase. Our model suggests that there exists a critical value $A_{crit} = 16/3^{3/2} \approx 3.0792$, below which separation is unlikely to facilitate the coalescence of the droplets. The predictions are in good agreement with available experimental data.

1. Introduction

The interactions between two or more droplets in flow play an important part in multiphase systems, such as emulsions in which the size distribution is determined by a balance between droplet breakup and coalescence. For example, in order to facilitate the creation of stable emulsions or to enhance the destruction of emulsions, we need to better understand the dynamical features of flows that cause coalescence. Much previous research has focused on drop deformation in unbounded flows (Rallison 1984; Stone 1994), interactions significant in the flow of dense suspensions (Loewenberg & Hinch 1997), local deformations that are precursors to coalescence (Jones & Wilson 1978; Nemer *et al.* 2004; Aarts & Lekkerkerker 2008) and dynamics of the coalescence process (e.g. Eggers, Lister & Stone 1999). In this paper we are motivated by recent experiments illustrating coalescence in bounded configurations when two drops are effectively pulled apart (Bremond, Thiam & Bibette 2008).

† Email address for correspondence: has@seas.harvard.edu

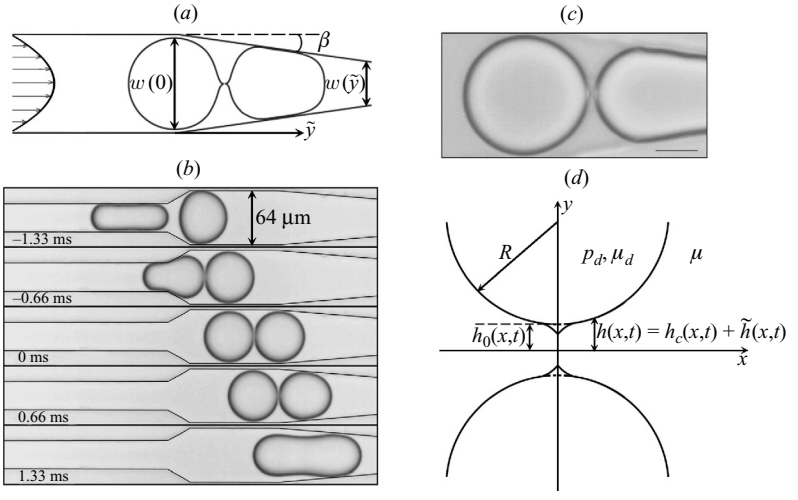

FIGURE 1. (*a*) Schematic of two droplets deforming and separating while moving through a smoothly constricting channel. (*b*) Time-sequenced images from experiments by Bremond *et al.* (2008) for droplets with radii 30 μm. The stresses resulting from separation create two facing nipples, which facilitate coalescence. (*c*) A close-up of an experiment showing the formation of two facing nipples prior to coalescence. The scale bar is 20 μm. (*d*) Schematic of the coordinate system for describing the region between two separating droplets. The undeformed circular shape $h_c(x, t)$ is indicated by the dotted curve.

Experimental results have shown that coalescence can occur when two deformable droplets move past one another in two-dimensional shear flow (Yoon *et al.* 2005). Also, Yoon *et al.* (2007) calculated numerically the extrusion formed as two nearly spherical droplets move apart in axisymmetric flow and suggested qualitatively that coalescence may occur; Loewenberg & Hinch (1997) made similar remarks for droplets in shear flow. This observation is supported by Manica *et al.* (2008) who suggested through both experiment and numerical modeling that when deformed by separating the interfaces with the intention of increasing its thickness, a thin film can become thinner. In addition, microfluidic experiments by Bremond *et al.* (2008), sketched in figure 1(*a*) and shown in figures 1(*b*)–1(*c*), demonstrate that two droplets, approximately circular in shape, generate facing nipple-like extrusions, which lead to coalescence during separation, not during collision.

Here, we present an analytical study of the microfluidic flow system utilized by Bremond *et al.* (2008). In § 2.1, we approximate the time-dependent droplet deformation due to droplet separation. The steps in our analysis follow the theme of other studies on the small deformation of droplets. First, we calculate the base flow for an undeformed shape. The stresses generated by such flows are then used in the normal stress balance to determine the perturbed shape of the droplet; these ideas are similar in approach to analyses of droplet deformation in unbounded linear flows, such as in Taylor (1934) and Barthés-Biesel & Acrivos (1973). With the coordinate system as shown in figure 1(*d*) in which the droplets have a separation distance $2h_0(t)$ and radius $R \gg h_0$, the typical length scale for flow along the gap between the droplets is $\ell \sim \sqrt{2Rh_0}$. The associated pressure reduction is then $\Delta p \approx \mu \dot{h}_0 R/h_0^2$, where $\dot{h}_0 = \mathrm{d}h_0/\mathrm{d}t$ is the time-dependent rate of separation of the droplets and μ is the viscosity of the continuous phase. The interface is then expected to deform with magnitude $\tilde{h}$ such that $\gamma \tilde{h}/\ell^2 \sim \Delta p$, where γ is the surface tension. Hence, by

scaling arguments, we expect the deformation $\tilde{h} = O(\mu \dot{h}_0 R^2/\gamma h_0)$. In § 2.2, we study how such shape deformations approach contact and suggest an approximate criterion for coalescence. Nevertheless, we recognize that the hydrodynamic approximations that we make become invalid in the last stages approaching coalescence, for which detailed numerical simulations are needed (Yoon *et al.* 2007; Manica *et al.* 2008). In § 3, we apply our results to the typical experimental system studied by Bremond *et al.* (2008). Finally, in § 4, we compare our results to the available experimental data from Bremond *et al.* (2008).

2. Theoretical model

We examine the simplified case in which droplets move through microchannels with height (in the z-direction) $2b$ that is much less than the width (in the y-direction) w. The undeformed droplets, circular in the xy-plane, have radius $R \approx w/2 > b$. In this limit, the fluid flow both around and between the droplets is primarily in the xy-plane. Thus, we expect the droplets to deform primarily in the xy-plane, and the smallest dimension b contributes only to an increased capillary pressure within the droplets. Consequently, we model the flow between two separating droplets as that between two slightly deformable cylinders.

Also, consistent with experiments, with a separation distance $2h_0(t)$ much smaller than the radius of the droplets, i.e. $h_0 \ll R$, the flow in the gap is controlled by the boundary condition at the interface. For the case of lubrication flows between two spherical droplets, Davis, Schonberg & Rallison (1989) have shown that the mobility of the interface depends on two dimensionless parameters h_0/R and μ/μ_d, where μ is the viscosity of the continuous phase, which fills the gap between the droplets, and μ_d is the viscosity of the droplets. We expect the features of their analysis to apply to our case of two nearly cylindrical droplets. For example, they determined that when the continuous phase has a much lower viscosity than the droplets ($\mu/\mu_d \ll \sqrt{h_0/R}$), the interface can be approximated as a no-slip boundary; we expect this limit to also apply when sufficient surfactant exists in the system. There is also an intermediate regime when $\sqrt{R/h_0} \gg \mu/\mu_d \gg \sqrt{h_0/R}$, where, although the interface is mobile, the lubrication approach yields results within a constant scaling factor C which depends on $(\mu/\mu_d)\sqrt{R/h_0}$. In the regime in which the continuous phase has much higher viscosity than the droplets ($\mu/\mu_d \geqslant \sqrt{R/h_0}$), it becomes necessary to consider the flow and the stresses inside the droplets. However, the experiments that we consider fall within the first two cases (e.g. the systems used by Bremond *et al.* 2008 have $\mu/\mu_d \approx 3$), allowing us to focus on the fluid motion in the gap region and the associated stresses. Although boundary conditions are important to coalescence (Yoon *et al.* 2007), because we focus on a lubrication model for the droplets' approach to contact resulting from the separation of their centres of mass, we believe the above assumptions to still be applicable.

2.1. *Droplet deformation analysis*

We now choose the origin of the coordinate system $x = 0$ to be within the gap between the two circular droplets, which have a separation distance of $2h_0(t)$, as shown in figure 1(d). We assume the droplets to be separating at a rate $2\dot{h}_0(t)$, where the dot denotes the time derivative. The associated flow creates a stress field that deforms the droplets from the initial circular shape. To determine the deformed shape of the droplets and, hence, the potential for droplet to coalesce, we start by determining the pressure p in the region between the two separating droplets. To simplify the

problem, we first model the droplets as circles, and since $h_0(t) \ll R$, we approximate the droplet shape in the gap region to be parabolic with a typical length scale $\sqrt{2Rh_0}$ in the x-direction. Through a lubrication analysis, which assumes the flow field to be quasi-steady ($p \to p_0$ as $x \gg \sqrt{2Rh_0}$), we then find

$$p(x,t) - p_0 = -\frac{C\mu \dot{h}_0(t) R}{2h_0(t)^2 \left(1 + \frac{x^2}{2Rh_0(t)}\right)^2}, \tag{2.1}$$

where p_0 is the reference pressure (Leal 1992). Here, the constant C depends on μ/μ_d; in the limit $\mu/\mu_d \to 0$, $C = 3$ (Davis *et al.* 1989). From this result, we can see that when the separation between the droplets increases, e.g. $\dot{h}_0(t) > 0$, the pressure decreases within the region between the two droplets, thus driving deformation towards coalescence as suggested qualitatively by Yoon *et al.* (2007), Bremond *et al.* (2008) and Manica *et al.* (2008). Our subsequent analysis neglects the effect due to van der Waals interactions, which are of importance only at significantly smaller length scales.

Here, we will analytically obtain the deformation of the droplet over time as well as identify the conditions that lead to contact. The curvature $\kappa(x,t)$ of the surface of the droplet results from the difference between the pressure outside of the droplet, p, and the pressure within the droplet, p_d, via the relation $p - p_d = \gamma\kappa(x,t)$, since within the limits appropriate for lubrication analysis, viscous stresses can be neglected in the normal stress balance. This description is self-consistent, since all perturbations to the initial undeformed shape occur in the narrow region between the two droplets, where the lubrication analysis is applied. Therefore, at the interface, (2.1) becomes

$$p_0 - p_d - \frac{C\mu \dot{h}_0(t) R}{2h_0(t)^2 \left(1 + \frac{x^2}{2Rh_0(t)}\right)^2} = \gamma\kappa(x,t). \tag{2.2}$$

Although we model the undeformed droplets to be two-dimensional, in the normal stress balances, we need to account for the curvature contribution in the yz-plane. Our sign convention for curvature is chosen with respect to the coordinate system shown in figure 1(d), where the origin is the mid-point between the centre of the two droplets, outside of the droplets. Hence, constricted in the z-direction to a height of $2b$, an undeformed droplet with radius R in the xy-plane has curvature $\kappa_c = -(\pi/4R) - 1/b$, where the factor of $\pi/4$ was derived by Park, Gorell & Homsy (1984) and Park & Homsy (1984). Therefore, $p_d - p_0 = \gamma((\pi/4R) + 1/b)$, and (2.2) reduces to

$$-\left(\frac{\pi}{4R} + \frac{1}{b}\right) - \frac{C\mu \dot{h}_0(t) R}{2\gamma h_0(t)^2 \left(1 + \frac{x^2}{2Rh_0(t)}\right)^2} = \kappa(x,t). \tag{2.3}$$

Because $b \ll w \approx R$, deformations in the yz-plane can be neglected as a first approximation, since they are expected to be smaller than those in the xy-plane by $O(b/R)$. Thus, we assume that curvature in the yz-plane, $-1/b$, remains constant, and accounting for the curvature in the xy-plane, $\kappa(x,t)$ can be written as

$$\kappa(x,t) = -\frac{1}{b} + \frac{\pi}{4}\frac{\partial}{\partial x}\left(\frac{\frac{\partial h}{\partial x}}{\sqrt{1 + \left(\frac{\partial h}{\partial x}\right)^2}}\right). \tag{2.4}$$

Although we can now integrate (2.3) and (2.4), we have found it helpful to focus first on simplifying κ by treating curvature changes as the result of perturbations

to the circular shape. Because the deformation of the droplet is small compared to the size of the droplet, R, we can apply the method of domain perturbation to determine the shape of the deformed droplet. We let $h(x,t) = h_c(x,t) + \tilde{h}(x,t)$, where $h_c(x,t)$ describes the shape of the unperturbed circular droplet (figure 1*d*) and $\tilde{h}(x,t)$ describes the separation-induced deformation as a small correction to $h_c(x)$. Then, since $h_0 \ll R$ and $|\mathrm{d}h_c/\mathrm{d}x| \ll |\partial\tilde{h}/\partial x|$ in the region of lowest pressure and largest deformation, we obtain an approximate equation for curvature,

$$\kappa(x,t) = \kappa_c + \tilde{\kappa}(x,t) \approx \kappa_c + \frac{\pi}{4}\frac{\partial^2\tilde{h}}{\partial x^2} \tag{2.5}$$

By substituting (2.5) into (2.3), we arrive at the normal stress balance,

$$\frac{\partial^2\tilde{h}}{\partial x^2} = -\frac{2C\mu\dot{h}_0(t)R}{\pi\gamma h_0(t)^2\left(1+\frac{x^2}{2Rh_0(t)}\right)^2}. \tag{2.6}$$

At this point, we non-dimensionalize (2.6) by using $X = x/\sqrt{2Rh_0(t)}$ and $H = \tilde{h}/D$ with $D = 2C\mu\dot{h}_0(t)R^2/\pi\gamma h_0(t)$. We then integrate with the condition that as $X \to \infty$, $\partial H/\partial X \to 0$ to obtain

$$\frac{\partial H}{\partial X} = -\left[\frac{X}{1+X^2} + \arctan(X) - \frac{\pi}{2}\right]. \tag{2.7}$$

Finally, we integrate (2.7) with the condition that at $X \to \infty$, $H \to 0$ to obtain the (similarity) solution for the deformation,

$$H(X) = -\left[X\left(\arctan(X) - \frac{\pi}{2}\right) + 1\right]. \tag{2.8}$$

This result, $H = \tilde{h}/D < 0$, is consistent with the assumption that separation-induced deformations favour possible contact between two droplets.

Using this solution for deformation, we determine the approximate deformed shape of the droplet $h(x,t) = h_c(x,t) + \tilde{h}(x,t)$ to be

$$h(x,t) = R + h_0(t) - \sqrt{R^2 - x^2} - \frac{2C\mu\dot{h}_0(t)R^2}{\pi\gamma h_0(t)} \times \left[\frac{x}{\sqrt{2Rh_0(t)}}\left(\arctan\left(\frac{x}{\sqrt{2Rh_0(t)}}\right) - \frac{\pi}{2}\right) + 1\right]. \tag{2.9}$$

This result shows that since the droplets are moving apart from one another, $\dot{h}_0(t) > 0$, deformation grows with time and is most prominent near $x < \sqrt{2Rh_0(t)}$. In addition, (2.9) agrees with our initial prediction for the magnitude of deformation $\tilde{h} = O(\mu\dot{h}_0R^2/\gamma h_0)$, which we arrived at in § 1 through a scaling argument.

2.2. *Approximate condition for droplet contact*

Although our analysis in the previous section assumes $|\tilde{h}(x,t)| \ll h_0(t)$, as set as precedent by other applications of domain perturbation, we now consider $|\tilde{h}(x,t)| \to h_0(t)$. According to (2.8), the largest deformation, or the deformation magnitude, occurs at $X = 0$, where $|H| = 1$. Thus, we find the dimensional magnitude of the deformation $\tilde{h}_{max}(t)$ to be

$$\tilde{h}_{max}(t) = \frac{2C\mu\dot{h}_0(t)R^2}{\pi\gamma h_0(t)}. \tag{2.10}$$

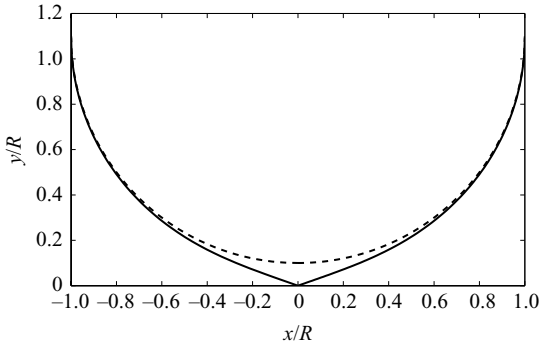

FIGURE 2. Typical shape of a droplet deformed by the separation of the droplet pair. The dotted line indicates the undeformed shape, while the solid line indicates the deformed shape at time of contact. Half of the separation distance of the undeformed droplets at time of contact is $h_0(t_c) = 0.1R$.

Within this lubrication model, in order for contact to occur, the magnitude of the deformation must equal half of the distance of separation between the two droplets. In other words, at the time of contact t_c, $h_0(t_c) = \tilde{h}_{max}(t_c)$, which leads to the condition

$$[h_0(t_c)]^2 = \frac{2C\mu \dot{h}_0(t_c) R^2}{\pi\gamma}. \tag{2.11}$$

The conditions shown in (2.10) and (2.11) are applicable for any time-evolution equation for droplet separation, $h_0(t)$, as long as $h_0(t) > 0$. With this additional information, we can determine the time of contact with (2.11). A specific example based on the experiments by Bremond *et al.* (2008) will be discussed in the next section.

Based on these results, the approximate deformed shape at the time of contact, t_c, is

$$\frac{h(x,t_c)}{R} = 1 + \frac{h_0(t_c)}{R} - \sqrt{1 - \left(\frac{x}{R}\right)^2} - \frac{h_0(t_c)}{R} \times \left[\frac{x/R}{\sqrt{2h_0(t_c)/R}}\left(\arctan\left(\frac{x/R}{\sqrt{2h_0(t_c)/R}}\right) - \frac{\pi}{2}\right) + 1\right]. \tag{2.12}$$

Figure 2 shows the shape of the deformed droplet at the time of contact, superimposed upon that of the undeformed droplet, for $h_0(t_c) = 0.1R$. As shown, the deformed shape near the point of contact is wedge-shaped with $h = (\pi/2^{3/2})\sqrt{h_0(t_c)/R}x$.

3. Application to the separation of two droplets in a linearly constricting channel

To simulate conditions of the experiments by Bremond *et al.* (2008), we first need to determine the appropriate time evolution of droplet separation. For the segment of the microchannel that linearly narrows with inclination angle β, as shown in figure 1(*a*), we can describe the width of the channel as $w(\tilde{y}) = w(0) - 2\tilde{y}\tan\beta$, where $\tilde{y}$ is along the length of the channel. We then apply conservation of mass $\langle u(0)\rangle w(0) = \langle u(\tilde{y})\rangle w(\tilde{y})$, where $\langle u(\tilde{y})\rangle$ is the average flow speed, to arrive at

$$\langle u(\tilde{y})\rangle = \frac{\langle u(0)\rangle}{1 - \frac{2\tilde{y}\tan\beta}{w(0)}}. \tag{3.1}$$

For $\tilde{y} \ll w(0)$, we approximate $\tilde{y} \approx \langle u(0)\rangle t$, and (3.1) becomes

$$\langle u(\tilde{y})\rangle - \langle u(0)\rangle \approx \frac{2\langle u(0)\rangle^2 \tan\beta}{w(0)} t. \tag{3.2}$$

We then assume that the droplets follow the flow of the continuous phase and use $\langle u(\tilde{y})\rangle = \mathrm{d}\tilde{y}/\mathrm{d}t$ to track the droplet movement. Therefore, $\langle u(\tilde{y})\rangle - \langle u(0)\rangle = 2\mathrm{d}h_0(t)/\mathrm{d}t$, and we find the separation velocity to be

$$\frac{\mathrm{d}h_0(t)}{\mathrm{d}t} = \frac{\langle u(0)\rangle^2 \tan\beta}{w(0)} t. \tag{3.3}$$

Initially, the two droplets have a separation of $2h_0(0)$ and zero separation velocity, since they start with the same constant velocity. We integrate (3.3) to arrive at $h_0(t) = h_0(0) + \alpha t^2$, where $\alpha = \langle u(0)\rangle^2 \tan\beta/2w(0)$ is the separation parameter that describes the two separating droplets. In the experiments by Bremond *et al.* (2008), $0.1\,\mathrm{m\,s^{-2}} < \alpha < 10\,\mathrm{m\,s^{-2}}$ (see § 4).

With this description of the time evolution of droplet separation, we can determine the conditions for systems like that used by Bremond *et al.* (2008), in which coalescence by droplet separation is demonstrated. Equations (2.10) and (2.11) become, respectively,

$$\tilde{h}_{max}(t) = \frac{4C\mu R^2 \alpha t}{\pi\gamma(h_0(0) + \alpha t^2)} \tag{3.4}$$

and

$$\left[1 + \left(t_c\sqrt{\frac{\alpha}{h_0(0)}}\right)^2\right]^2 = \frac{4C\mu R^2}{\pi\gamma}\frac{\alpha t_c}{[h_0(0)]^2}. \tag{3.5}$$

By non-dimensionalizing (3.4) and (3.5) with $T = t\sqrt{\alpha/h_0(0)}$ and $H_{max} = \tilde{h}_{max}/D_{max}$, where $D_{max} = (2C\mu R^2/\pi\gamma)\sqrt{\alpha/h_0(0)}$, we arrive, respectively, at

$$H_{max}(T) = \frac{2T}{1+T^2} \tag{3.6}$$

and

$$T_c^2 - \sqrt{AT_c} + 1 = 0, \qquad \text{where} \qquad A = \frac{4C\mu R^2 \alpha^{1/2}}{\pi\gamma[h_0(0)]^{3/2}}. \tag{3.7}$$

In the limit of $\mathrm{A} \gg 1$ in which $R \gg h_0(0)$, $A \sim T_c^{-1}$. Therefore, we estimate the contact time, t_c, as

$$t_c \approx \frac{\gamma[h_0(0)]^2}{\mu R^2 \alpha}. \tag{3.8}$$

Although approximate, these results illustrate the most important features of the time-dependent deformation of the separating droplets as well as the subsequent potential for coalescence. First, we can observe that without coalescence, the extruding deformation, with magnitude $H_{max}(T)$, initially grows rapidly with time until $T = 1$ and then retracts slowly, as figure 3 exhibits. Initially, viscosity effects dominate and create a pressure difference between the inside and the outside of the droplet capable of overcoming the surface tension effect, thus creating the nipple extrusion. As the droplets move further apart, viscous effects decrease until they are no longer capable of overcoming the surface tension effect, which restores the droplet's spherical shape. Therefore, if near contact between two droplets is not achieved within this initial window of time, i.e. $T \leqslant 1$ or $t \leqslant \sqrt{h_0(0)/\alpha}$, coalescence will be unlikely to happen,

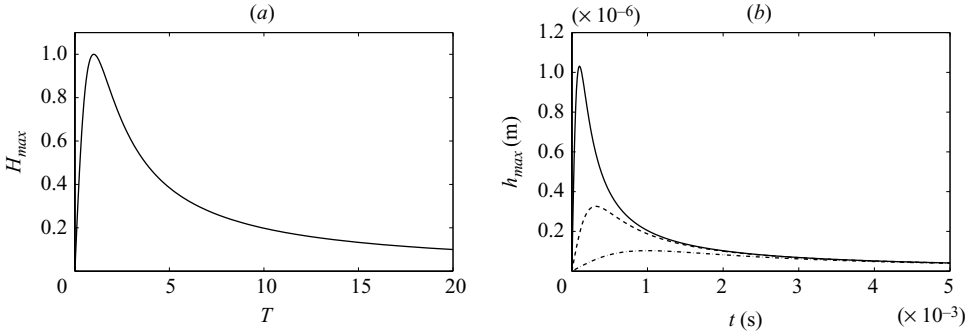

FIGURE 3. (*a*) Non-dimensional maximum deformation $H_{max} = |h_{max}|[\pi\gamma/(2C\mu R^2)]\sqrt{h_0(0)/\alpha}$ as a function of non-dimensional time $T = t\sqrt{\alpha/h_0(0)}$. (*b*) Dimensional maximum deformation $|h_{max}|(m)$ as a function of time t(s) for $\alpha = 0.1\,\mathrm{m\,s^{-2}}$ (dash-dotted line), $\alpha = 1\,\mathrm{m\,s^{-2}}$ (dashed line) and $\alpha = 10\,\mathrm{m\,s^{-2}}$ (solid line) with $h_0(0) = 0.1\,\mu\mathrm{m}$, $R = 30\,\mu\mathrm{m}$, $\mu = 3 \times 10^{-3}\,\mathrm{Pa\,s}$, $\gamma = 50 \times 10^{-3}\,\mathrm{N\,m^{-1}}$ and $C = 3$, based on experimental values from Bremond *et al.* (2008).

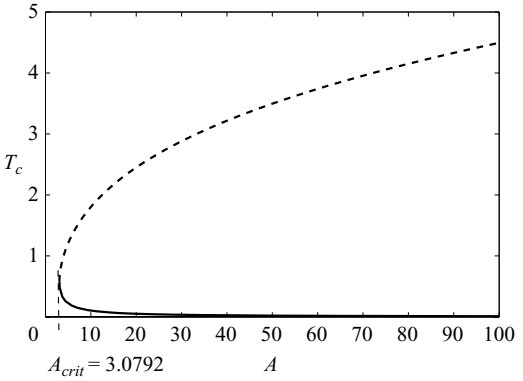

FIGURE 4. Non-dimensional time of contact for the extruding phase, $T_c = t_c\sqrt{\alpha/h_0(0)}$, as a function of the non-dimensional parameter, $A = 4C\mu R^2\alpha^{1/2}/\pi\gamma[h_0(0)]^{3/2}$ (solid line). The dashed line represents the physically unrealistic scenario in which coalescence occurs during the retracting phase.

since the nipple will retract while the gap between the droplets continues to grow. This result corresponds qualitatively with the three-dimensional simulations performed by Yoon *et al.* (2007) in their figure 25.

We examined this critical point more explicitly by illustrating that the contact time, T_c, increases as the non-dimensional parameter, A, decreases, as shown in figure 4. The dotted line represents the physically unrealistic solution in which $\tilde{h}(t) = h_0(t)$ while the nipple is retracting, not extruding; this scenario is unlikely because we expect the droplets to typically coalesce upon first contact, which occurs during the extruding phase. We thus identify $A_{crit} = 16/3^{3/2} \approx 3.0792$ and $T_{crit} = 1/\sqrt{3} \approx 0.5774$, below which the two droplets do not come into contact. This approximate limit for near contact can be attributed to many reasons. As γ increases, μ decreases or R decreases, the restoring surface tension effects increase relative to the deformation, inducing viscous effects and leading to decreased deformation magnitude, which subsequently cannot match or exceed the separation magnitude. In addition, when $h_0(0)$ increases, not only do the viscous effects decrease, but the separation distance also increases. On the

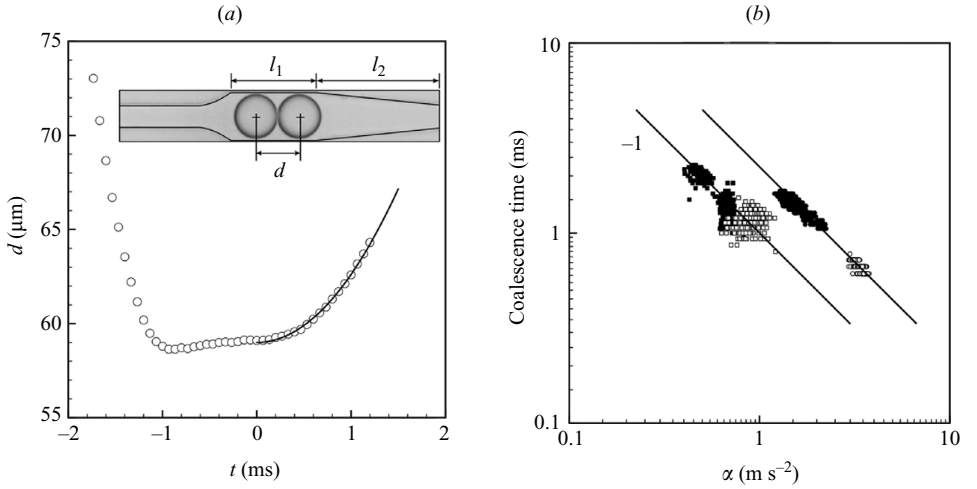

FIGURE 5. (*a*) Experimental data showing the time evolution of the distance d between the centres of mass of the two droplets. The origin of time is determined when the first droplet enters the region in which the channel begins to constrict. The continuous line represents the fit $d(0) + 2\alpha t^2$, $\alpha = 1.8\,\mathrm{m\,s^{-2}}$. Inset: Image of two droplets entering the linearly constricting channel. (*b*) Coalescence time as a function of the separation parameter, α, for several experimental conditions (q_0 and q_w denote the oil and water flow rates, respectively): chamber 1, $q_o = 400\,\mu\mathrm{l\,h^{-1}}$, $q_w = 100\,\mu\mathrm{l\,h^{-1}}$ (●); chamber 2, $q_o = 400\,\mu\mathrm{l\,h^{-1}}$, $q_w = 100\,\mu\mathrm{l\,h^{-1}}$ (○); chamber 1, $q_o = 200\,\mu\mathrm{l\,h^{-1}}$, $q_w = 50\,\mu\mathrm{l\,h^{-1}}$ (■); chamber 2, $q_o = 200\,\mu\mathrm{l\,h^{-1}}$, $q_w = 50\,\mu\mathrm{l\,h^{-1}}$ (□).

other hand, when α decreases, although the separation increases more slowly, the rate of change of the growth of the distance between the droplets is directly correlated with the magnitude of the deformation generated; hence, decreasing α ultimately decreases the deformation magnitude.

4. Comparison with experimental results

In the experiments by Bremond *et al.* (2008), pairs of water-in-oil (hexadecane) droplets are generated by splitting a train of single droplets formed by a flow-focusing module. The water flow rate q_w as well as the oil flow rate q_o are controlled by two syringe pumps (phd 2200, Harvard Apparatus). The complete history of a droplet pair is recorded with a high-speed camera (Fastcam-X 1024, Photron) mounted on an inverted microscope (TE300, Nikon). Many thousands of coalescence events are recorded and automatically analysed using image-processing programs developed with MATLAB.

As previously discussed, the droplets collide in the expanding portion of the channel and separate in the constricting portion of the channel (figure 1*a*). This experimental system is characterized by two lengths: ℓ_1, the length of the channel in which the width is constant, and ℓ_2, the length of the constricting portion. Two configurations were used: $\ell_1 = 60\,\mu\mathrm{m}$ and $\ell_2 = 200\,\mu\mathrm{m}$ (chamber 1); $\ell_1 = 120\,\mu\mathrm{m}$ and $\ell_2 = 200\,\mu\mathrm{m}$ (chamber 2).

Previously, we prescribed $h_0(t) = h_0(0) + \alpha t^2$ to describe the separation motion of the droplets in a linearly constricting channel. The results from Bremond *et al.* (2008) support this functional form as shown in figure 5(*a*). Because the resolution of the optics involved in imaging the experiments does not allow for accurate assessment of $h_0(t)$, the results are reported in terms of the distance, $d(t)$, between the centre of

mass of the two droplets. Since we assume R to be constant and $h_0(t) = (d(t) - 2R)/2$, by fitting the data to the curve, $d(t) = d(0) + 2\alpha t^2$, we can estimate α without direct measurement of h_0. For the results in figure 5(*a*), we find $\alpha = 1.8\,\mathrm{m\,s^{-2}}$.

Next, we examined the relationship between the separation parameter, α, and the experimentally measured time of coalescence, which we assume follows our estimate for time of contact, t_c. Equation (3.8) predicts $t_c \propto \alpha^{-1}$, which is in good agreement with the trends shown in figure 5(*b*). The dispersion of the data likely results from not incorporating the effects of R and $h_0(0)$, as suggested by (3.8). In our experimental system, variations in R lead to significant variations in h_0, which, due to the limitation of the resolution of the optics involved, could not be accurately evaluated. Consequently, the effects of both R and $h_0(0)$ could not be assessed. Nevertheless, we note that the data shown in figure 5 with $t_c \simeq 10^{-3}$ s, when interpreted using (3.8), are consistent with $h_0(0) \simeq 0.3\,\mu\mathrm{m}$. Future work can focus on developing experiments to more accurately determine the values for $h_0(0)$. We believe that by incorporating the effects due to $h_0(0)$, we can better assess the details of our theoretical model.

5. Conclusion

We have analytically studied the near-contact phase of the phenomenon of droplet coalescence during separation by employing a lubrication analysis in combination with the method of domain perturbation. Our general results for the magnitude of deformation, $h_{max}(t)$, as well as the general shape deformation are in good agreement with the experimental results and the result from dimensional analysis. For a linearly constricting channel in which the half-separation distance follows $h_0(t) = h_0(0) + \alpha t^2$, we found that for typical systems in which $R \gg h_0(0)$ and $A = 4C\mu R^2\alpha^{1/2}/\pi\gamma[h_0(0)]^{3/2} \gg 1$, the time of contact, t_c, is proportional to α^{-1}; this finding agrees with the experimental results by Bremond *et al.* (2008). In addition, for such systems, there exists a critical parameter value, $A_{crit} = 16/3^{3/2} \approx 3.0792$, below which the separation-driven droplet deformations are unlikely to bridge the separation distance between the two droplets. We believe that these ideas are applicable to separation-driven contact of other deformable systems. More insight on the evolution of film profile can be obtained from numerical simulations based on the full thin-film lubrication equations (e.g. Manica *et al.* 2008) or, more thoroughly, from boundary integral simulations of the complete two-fluid flow problem.

We acknowledge Abdou Rachid Thiam for his contribution to the experiments along with Jens Eggers and Jacy Bird for helpful conversations. We thank Gary Leal for detailed feedback that improved our paper. We also thank the Harvard MRSEC (DMR-0213805) for partial support of this research.

REFERENCES

Aarts, D. G. A. L. & Lekkerkerker, H. N. W. 2008 Droplet coalescence: drainage, film rupture and neck growth in ultralow interfacial tension systems. *J. Fluid Mech.* **606**, 275–294.

Barthés-Biesel, D. & Acrivos, A. 1973 Deformation and burst of a liquid droplet freely suspended in a linear shear field. *J. Fluid Mech.* **61**, 1–21.

Bremond, N., Thiam, A. R. & Bibette, J. 2008 Decompressing emulsion droplets favors coalescence. *Phys. Rev. Lett.* **100**, 024501.

Davis, R. H., Schonberg, J. A. & Rallison J. M. 1989 The lubrication force between two viscous drops. *Phys. Fluid* A **1**, 77–81.

Eggers, J., Lister, J. R. & Stone, H. A. 1999 Coalescence of liquid drops. *J. Fluid Mech.* **401**, 293–310.

Jones, A. F. & Wilson, S. D. R. 1978 The film drainage problem in droplet coalescence. *J. Fluid Mech.* **87**, 263–288.

Leal, L. G. 1992 *Laminar Flow and Convective Transport Processes.* Butterworth-Heinemann.

Loewenberg, M. & Hinch, E. J. 1997 Collision of two deformable drops in shear flow. *J. Fluid Mech.* **338**, 299–315.

Manica, R., Conner, J. N., Clasohm, L. Y., Carnie, S. L., Horn, R. G., & Chan, D. Y. C. 2008 Transient responses of a wetting film to mechanical and electrical perturbations. *Langmuir* **24**, 1381–1390.

Nemer, M. B., Chen, X., Papadopoulos, D. H., Blawzdziewicz, J. & Loewenberg, M. 2004 Hindered and accelerated coalescence of drops in Stokes flow. *Phys. Rev. Letters* **92**, 114501.

Park, C.-W., Gorell, S. & Homsy, G. M. 1984 Two-phase displacement in Hele–Shaw cells: experiments on viscously driven instabilities. *J. Fluid Mech.* **141**, 257–287.

Park, C.-W. & Homsy, G. M. 1984 Two-phase displacement in Hele–Shaw cells: theory. *J. Fluid Mech.* **139**, 291–308.

Rallison, J. M. 1984 The deformation of small viscous drops and bubbles in shear flows. *Annu. Rev. Fluid Mech.* **16**, 45–66.

Stone, H. A. 1994 Dynamics of drop deformation and breakup in viscous fluids. *Annu. Rev. Fluid Mech.* **26**, 65–102.

Taylor, G. I. 1934 The formation of emulsions in definable fields of flow. *Proc. R. Soc. Lond.* A **146**, 501–523.

Yoon, Y., Baldessari, F., Ceniceros, H.D. & Leal, L. G. 2007 Coalescence of two equal-sized deformable drops in an axisymmetric flow. *Phys. Fluid* **19**, 102102.

Yoon, Y., Borrell, M., Park, C. C. & Leal. L. G. 2005 Viscosity ratio effects on the coalescence of two equal-sized drops in a two-dimensional linear flow. *J. Fluid Mech.* **525**, 355–379.